PHYSICS OF SPACE PLASMA (1998), Number 15

Polar Plasma Wave Observations in the Auroral Region and Polar Cap

J. D. Menietti, T. F. Averkamp, D. L. Kirchner, J. S. Pickett, A. M. Persoon, and D. A. Gurnett

Department of Physics and Astronomy, The University of Iowa, Iowa City, IA 52242 USA

Abstract. Auroral kilometric radiation (AKR), sometimes associated with auroral myriametric radiation (AMR), has been observed by the plasma wave instrument on board Polar on almost every northern hemisphere pass. High spectral resolution plots of the AKR obtained by the wideband receiver of the plasma wave instrument on board the spacecraft often show discrete, negative-slope striations each extending over a period of several seconds. A preliminary survey of over 4000 spectrograms (each for 48 seconds of data) indicates that the striations are seen in the northern hemisphere near apogee about 5% of the time. The frequency range is 40 kHz < f < 100 kHz, but a few observations of signatures have been made at higher frequency (f < 225 kHz). The frequency drift rates, R, are similar ranging from -9.0 kHz/sec < R < -1.0 kHz/sec. No data is currently available for perigee (southern hemisphere) passes. The paucity of positive-slope features may be due to the location of the satellite at altitudes well above the AKR source region. Past studies have suggested these features are due to AKR wave growth stimulated by the propagation of electromagnetic ion cyclotron waves travelling up (-R) or down (+R) the field line, through the source region. High-resolution waveform data from both Polar and FAST show the presence of solitary waves in the auroral region which may also be a source of these striations. AMR is seen as diffuse emission associated with, but at lower frequency than the AKR. Direction finding of these emissions is not conclusive, but for one case, they have a source region distinct from the magnetic field line containing the AKR source, but possibly associated with the auroral cavity density gradient.

1.0 Introduction and Background

1.1 Auroral kilometric radiation fine-structure

Gurnett et al. [1979] and *Gurnett and Anderson* [1981] using ISEE data, *Benson et al.* [1988] using DE-1 data, and *Morioka et al.* [1981] with EXOS-B data have all reported examples of auroral kilometric radiation (AKR) fine structure in both the ordinary and extraordinary modes indicating that AKR is emitted in discrete bursts lasting only a few seconds or less. Observed frequency drift rates of features are in the range 100 Hz/sec < R < 10's of kHz/sec. The bandwidth can be quite small (< 1 kHz). *Gurnett et al.* [1979] suggest that the drifting features may be due to rising and falling source regions. The fine structures include not only drifting features, but also discrete bands of near-monochromatic emission and other discrete features that are seen at the highest resolution available.

There are a number of theories which attempt to explain the source of the AKR fine structure observed. Such knowledge is necessary if we are to fully understand the details of the AKR generation mechanism. *Wu and Lee* [1979] have no doubt identified the general instability mechanism responsible for the emission, but as pointed out some years ago by *Melrose* [1986], the cyclotron maser mechanism would be an incomplete theory if it could not explain the time scales of wave growth associated with AKR fine structure. The signatures we address in this paper are a special subset of AKR fine structure. The features are structured striations in the AKR wideband data that appear on relatively few Polar northern hemispheric passes near apogee. The bandwidth of the fine structure, for instance, puts severe constraints on spatial growth rates as produced by the cyclotron maser instability. *Menietti et al.* [1996] have presented observations of possible stimulated AKR. In that paper impulsive wave generation and intrinsic velocity dispersion was discounted as a possible source of the discrete signatures observed in the wave data. *Menietti et al.* [1997] presented additional observations of the phenomena observed by Polar, and they presented a scenario for the generation of positive-slope signatures. In this paper we present the results of a survey of a portion of the Polar wideband data.

1.2 Auroral myriametric radiation

Another class of emissions that is sometimes seen and is associated with AKR is auroral myriametric radiation (AMR). The term Auroral Myriametric Radiation (AMR) was introduced by *Hashimoto et al.* [1994] who used Geotail observations to identify a rather diffuse radio emis-

sion at frequencies above the plasma frequency (a few kHz to ~ 60 kHz) that correlates well with enhancements of auroral kilometric radiation. Similar observations were reported by *Filbert and Kellogg* [1979] (IMP 6) and *Louarn et al.* [1994] (Galileo Earth 1 flyby) who refer to the emission as low frequency radiation (LFR). Recently *Hashimoto et al.* [1998] performed ray tracing of AMR based on GEOTAIL observations. Their results indicate that the emission is L-O mode and consistent with an auroral cavity source region (not a source near the gyrofrequency). We report here on AMR observations made by the Plasma Wave Instrument (PWI) on board the Polar spacecraft. All of these observations provide a starting point for further multi-satellite investigations that can lead to an increase in our understanding of polar magnetospheric plasma dynamics.

2.0 Instrumentation

The plasma wave instrument on board the Polar spacecraft contains two sweep-frequency receivers (SFR) that operate in the frequency range from about 25 Hz to 800 kHz. Three orthogonal electric antennas are available, two in the spin plane and one along the spin axis. A magnetic loop antenna and a triaxial magnetic search coil are used to detect magnetic signals. A signal correlator is used to measure the phase difference in degrees for parallel receivers that simultaneously detect signals from two antennas. In each of the five frequency bands, the frequency channels can be either logarithmically spaced (log step mode) or linearly spaced (linear step mode). In the log step mode, the frequency resolution varies from approximately 8% at 26 Hz to 3% at 800 kHz. The SFR sequentially advances through the frequency spectrum. In the lowest frequency band, 24-200 Hz, a full frequency spectrum can be obtained every 33 s in the log mode and every 66 s in the linear mode. Because of the wider bandwidths and hence faster response times, the higher frequency bands have faster sweep rates. From 12.5 to 800 kHz, a full frequency spectrum can be obtained every 2.4 s in the log mode and every 4.7 s in the linear mode. The SFR amplitude output ranges over a 100 dB dynamic range. In addition, a wideband receiver (WBR) provides high-time resolution over the frequency range 10 Hz to 600 kHz. The WBR has three normal modes of operation with bandwidths of 11, 22, and 90 kHz, and the base frequency can be adjusted to either 0, 125, 250, or 500 kHz.

3.0 Observations of Fine-structure Striations

In addition to DE-1 and Galileo, recent observations from Polar have also revealed AKR striations in similar frequency range and from regions over the polar cap and well above the AKR source region. Figure 1 is an nnexample of data obtained on March 13, 1996, when Polar was located over the polar cap. The striations are seen in the frequency range from about 65 kHz to perhaps over 100 kHz, although the upper frequency cutoff is not clear since the data is instrumentally restricted by the current operating mode. These stripes have a signature very similar to those observed both on Galileo and on DE-1. A typical slope was -5 kHz/sec.

3.1 Analysis

For an isolated example of AKR striations with relatively large frequency extent, *Menietti et al.* [1996] performed some detailed analyses. They considered two possible generation mechanisms: 1) impulsive stimulation of the entire AKR source region along a field line; 2) stimulated emission by a wave travelling up the magnetic field line. In the first scenario, the signature was considered to be produced by an intrinsic dispersion due to the source mechanism. For gyroemission, the wave group velocity decreases as the wave frequency approaches the local electron gyrofrequency, f_g, and this group velocity decreases as the gyrofrequency decreases. The authors first considered the possibility of impulsively stimulated emission at frequencies very near f_g at different points along the field line. They envisioned AKR generated with maximum growth rate at a frequency close to f_g such that $V_g/c << 1$. We refer the reader to that study for details. The authors concluded that impulsive stimulation by intrinsic dispersion of the wave group velocity along the field line was not feasible.

A statistical study of the occurrence of AKR fine structure observed on Polar plasma wave wideband data has been conducted. The amount of data is too large to com-

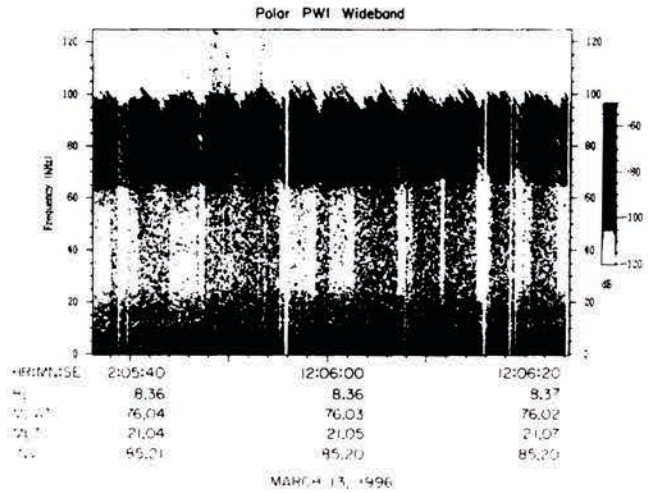

Figure 1. Wideband data obtained from the plasma wave instrument on board Polar as it was high over the northern polar cap on March 13, 1996. Note the numerous and quite intense examples of negative-slope stripes observed in the frequency range from 60 kHz < f < 100 kHz.

plete a manual analysis, so a sampling scheme was developed. All of the frequency-vs-time spectrograms for March 1996 were examined, each containing 48 seconds of data. These frames were examined for the presence of, frequency extent, and slope of striations. Striations were considered present if a series of linear stripe signatures persisted with relatively constant slope for about 10 seconds or more. Random individual signatures were not considered. This survey included 3709 48-second frames for a total of 2967 minutes of 90-kHz bandwidth spectrograms. Next, data from a series of essentially randomly selected days was sampled, for a total of 359 spectra. Using this approach, data from different locations and frequency ranges was analyzed. In all, over 4000 separate frames were analyzed. The results indicate that striations occur on about 5% of the frames. Almost all examples of the striations occurred for $f < 100$ kHz. Only a few cases (less than 10) were seen on frames covering the frequency range 125 kHz $< f <$ 225 kHz. Very little wideband data in the required 90 kHz bandwidth mode is available for Polar perigee (southern hemisphere) passes, so that it is not possible to draw any conclusions about the radial dependence of the striations at this time.

3.2 Wave stimulation

The bandwidth of the assumed gyroemission observed by *Menietti et al.* [1996] required that the source region extend several thousand kilometers along the field line. The observed signature lasted about 3.5 seconds, so the stimulating wave must have a group velocity along the field line of about 1000 km/sec. The striations for the observations made by DE-1 and Polar would require similar group velocities within a factor of 2 or 3. There are a number of candidates for such waves which have been observed regularly at frequencies near and below both the hydrogen and oxygen ion cyclotron frequencies (cf. *Gurnett et al.*, 1984). These emissions include whistler mode, Alfvén ion cyclotron waves, and electromagnetic ion cyclotron (EMIC) waves. *Menietti et al.* [1996] showed how at mid-auroral altitudes the most likely candidate for waves with group velocities in the correct range is the EMIC wave.

In order to produce the negative slope of the stripe it is necessary that the wave travel up the field line from larger to smaller gyrofrequencies. *Lin et al.* [1989] have shown that auroral electron beams with energies of several keV are likely sources of free energy for EMIC waves generated along auroral field lines. EMIC waves could propagate up the field line until they reached the ion cyclotron frequency, f_{ci}, where propagation would cease. The waves could propagate down the field line to the ionosphere and reflect at the point where the density gradient becomes very large (at altitudes of several hundred kilometers) [cf. *Temerin et al.*, 1986]. As discussed in *Lin et al.* [1989], electron beams are commonly observed in the auroral region with energies in the range of several keV can excite EMIC waves via Landau resonance. Thus the direction of propagation of the EMIC waves depend on the direction of the electron beams. Recently *McFadden et al.* [1998] have reported observations of strong wave-particle interactions between energetic electrons and H+ EMIC waves in inverted-V arcs. These occur in strong upward current regions with intense down-going electron fluxes.

Depicted in the cartoon of Figure 7 of *Menietti et al.* [1997] is a source of EMIC waves within the AKR source region. As mentioned above, the EMIC waves are envisioned to be generated by field-aligned plasma beams, which are produced by the field-aligned electric field. *Temerin et al.* [1986] have argued that the source of EMIC waves responsible for the flickering aurora are located near the bottom of the acceleration region where one would expect to find precipitating electron beams necessary to satisfy the cyclotron resonance condition for downward propagating EMIC waves. In the case depicted in Figure 7 of *Menietti et al.* [1997] upward propagating EMIC waves are seen near the top of the acceleration region, in the lower-frequency AKR source region. This is required by the observations which show that the AKR striations are observed in the lower frequency range of the AKR for $f < 100$ kHz. These waves might then stimulate the growth of AKR. The process by which the stimulation of AKR is accomplished is not known, but could involve local modification of the ratio of the plasma frequency to gyrofrequency, f_p/f_g, which strongly controls the generation of AKR.

4.0 Auroral Myriametric Radiation Direction Finding

An example of auroral myriametric radiation is shown in the frequency versus time spectrogram of Figure 2. The emission is seen in the electric field data (magnetic field data not shown) as a rather diffuse emission distinct from and at lower frequencies than the associated AKR.

For direction finding by PWS on board Polar, a signal correlator is used to measure the phase difference in degrees for parallel receivers that simultaneously detect signals from two antennas. With this information the direction to the emission source can be determined.

During the time of our observations of AMR, the E_z antenna (along the spacecraft spin axis) and the magnetic loop antenna (receiving signals in the spacecraft spin plane) were selected. The signal phase delay between these two antennas was then measured as a function of spacecraft spin angle. We have assumed circularly polarized emission and used the approach described in the past by *Mellott et al.* [1984] and *Calvert* [1985] for analysis of DE-1 plasma wave data. The approach used to perform phase-delay direction finding of the Polar plasma wave data is different from that used for DE-1, because for the case of Polar only an electric (E_z) and magnetic (B_L)

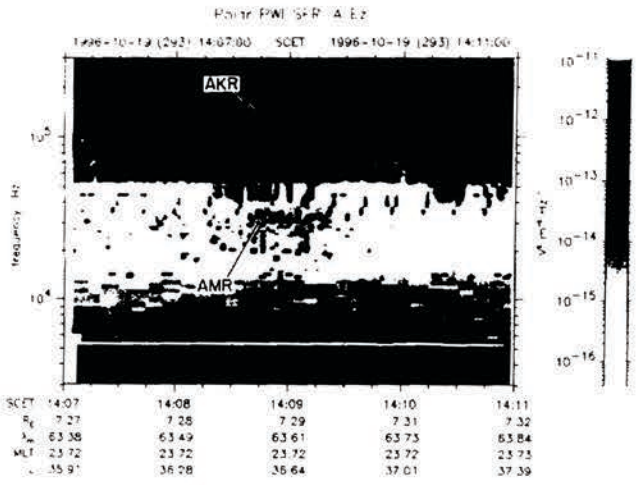

Figure 2. Frequency-versus-time spectrogram of the PWI electric field intensity is displayed for an example of diffuse AMR emission on day 293 of 1996. The AKR and AMR signals are indicated.

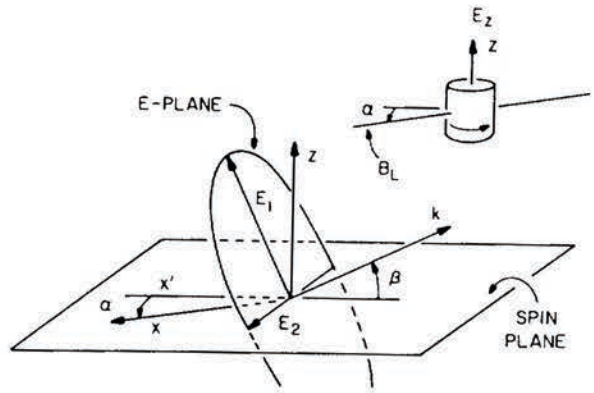

Figure 3. The geometry for reception of an elliptically polarized wave by the spacecraft E_z and B_L antennas, showing the waves's E-plane, its propagation direction **k** (at an angle β with respect to the satellite spin plane), and its orthogonal electric field components E_1 and E_2. The magnetic components of the wave are not shown.

antenna are available for phase analysis, rather than two electric antennas as was the case with DE-1. The geometry is as shown in Figure 3. The analysis can yield the direction to the source, but not the polarization of the signal, which will be ambiguous in general.

Consider an orthogonal coordinate system $(\mathbf{x_1}, \mathbf{x_2}, \mathbf{x_3})$. Following *Boyd and Sanderson* [1969] we write a general expression for a transverse, elliptically polarized, plane electromagnetic (EM) wave propagating in the $\mathbf{x_1}$-direction (along **k**) as

$$\mathbf{E}(x_1,t) = (E_{1_o}\,\mathbf{x_2} + i\,E_{2_o}\,\mathbf{x_3})\exp[i(kx_1-\omega t)] \quad (1)$$
$$\mathbf{B}(x_1,t) = (B_{1_o}\,\mathbf{x_2} + i\,B_{2_o}\,\mathbf{x_3})\exp[i(kx_1-\omega t+\pi/2)]$$

where E_{1_o}, E_{2_o}, B_{1_o}, and B_{2_o} are real quantities.

If the spacecraft axes are (x,y,z), from Figure 3 we can write

$$E_z = E_1 \cos\beta \quad (2)$$
$$B_x = B_1 \sin\beta\cos\alpha + B_2 \sin\alpha$$

where E_1, E_2, B_1, and B_2 are complex amplitudes, thus,

$$B_x/E_z = (\sin\alpha/\cos\beta)\,[B_1 \sin\beta/(E_1 \tan\alpha) + B_2/E_1]$$

From equation (1) we obtain

$$B_x/E_z = (\sin\alpha/\cos\beta)[(i)\sin\beta\; B_{1_o}/(\tan\alpha\; E_{1_o})\;\; B_{2_o}/E_{1_o}] \quad (3)$$

Following *Oya and Morioka* [1983] and *Calvert* [1985] we identify $\tan(\phi)$, where ϕ is phase angle, as the ratio of the imaginary to real parts of equation (3), i.e.,

$$\cot(\phi) = (\; B_{2_o}/B_{1_o})\tan\alpha/\sin\beta \quad (4)$$

By plotting the measured phase difference versus satellite spin angle α, we obtain a curve that can be fit to determine the direction to the source. In our case, we assume the emission is circularly polarized, so that $B_{z_o}/B_{y_o} = 1$ and the problem becomes one of a least-squares fit to the two parameters α_o and β where α_o is the satellite spin angle when the phase delay is 90°.

4.1 AMR direction finding results

We have determined the direction to the source for 4 cases of AMR where the signal strengths were large enough to obtain reasonable results. The limiting signal strength is that of the magnetic loop antenna, which is typically small for electromagnetic emission because of receiver sensitivity. In Figure 4 we show the directions to the source projected into the GSE z-x (top panel) and x-y (bottom panel) planes for day 96/293, one of the 4 cases studied. The error associated with these measurements is due to calibration errors (estimated at $< 2°$ for $f > 10$ kHz) and statistical errors associated with the data analysis. The latter errors are case dependent and for the case shown in Figure 4, we obtained a standard deviation of about 13.7°. Although the statistical errors are larger than desired, it is clear that the AMR source is not along the magnetic field line containing the AKR source. The directions to the AMR and AKR source regions are calculated to differ by more that 40°, which is much larger than the estimated error. For each of the other 3 examples of AMR emission, the direction to the source region was typically calculated to be just about as far away from the direction to the AKR source as the statistical error in the calculation. Thus, for these other 3 cases, the model of *Louarn et al.* [1994] and the model suggested by *Hashimoto et al.* [1998] are both consistent with the data. Only in

the case shown in Figure 4 does it appear that the source region is not associated with the active AKR magnetic field line.

5.0 Summary and Conclusions

5.1 AKR fine structure

Unusual striations in the fine structure of AKR are observed above the source region on about 5% of the northern hemisphere passes of the Polar spacecraft. The frequency range is from ~ 40 kHz to ~ 100 kHz, with a few cases for f < 225 kHz. These studies were conducted for a sample of over 4000 48-second spectrograms. The striations are observed exclusively with negative slope at the lower range of AKR frequencies. We suggest that the negative-slope striations are produced by stimulation of the source region by electromagnetic plasma waves travelling away from Earth, through the AKR source region. A wave travelling up the magnetic field line with a group velocity of about 1000 km/sec would pass through the AKR source region (40 kHz < f < 65 kHz) in about 3.5 seconds, in agreement with the observations. The source of the upward propagating EMIC waves may be near the top of the acceleration region where the local gyrofrequency is less than about 100 kHz. Alternatively, the EMIC source region could extend below the acceleration region in which case downward EMIC waves which subsequently reflect at low altitude to propagate back up through the AKR source region might be the source of the AKR stripes. Positive-slope striations, alternatively, could be stimulated by downward propagating EMIC waves. These waves may be associated with AKR that propagates principally toward the Earth, and thus is not typically observed by a satellite above the AKR source region.

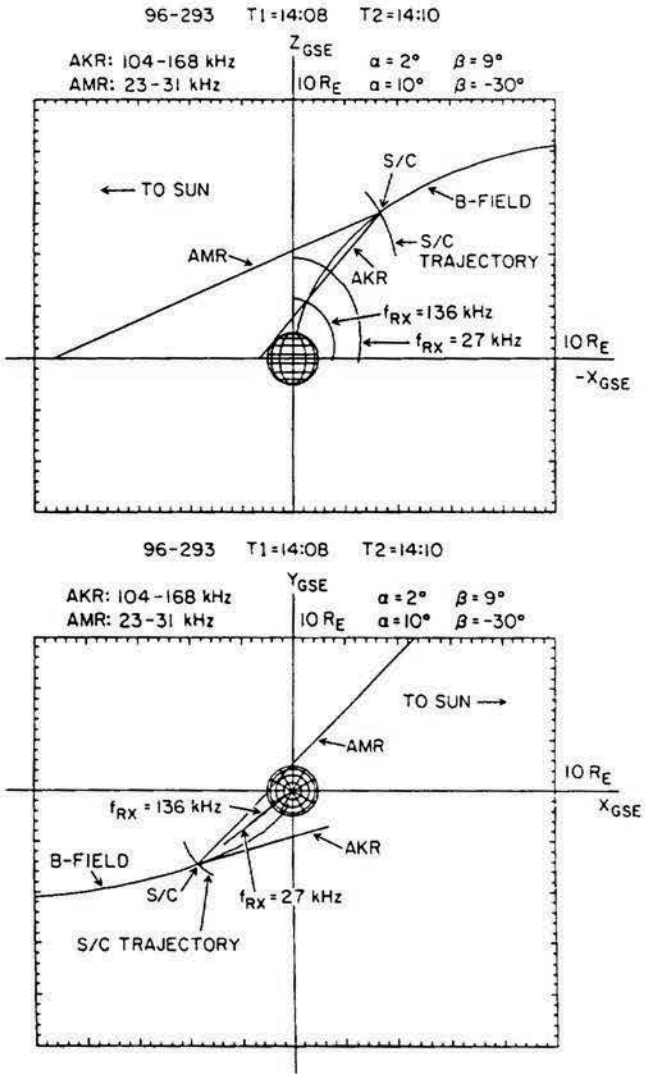

Figure 4. The calculated directions from the spacecraft to the AKR and AMR source regions for day 293 of 1996. The plots are 2-D projections in the GSE coordinate system, the Z-X plane (top) and the X-Y plane (bottom). The AMR is calculated for an observed frequency range of 23 to 31 kHz, and the most intense AKR was observed in the frequency range of 104 to 168 kHz.

The actual mechanism by which the AKR emission is stimulated has not been critically investigated, but we suggest that as the stimulating wave propagates through the AKR source region, it modifies the ratio f_p/f_g and/or the plasma distribution in pitch angle or energy. As the time and frequency resolution of plasma wave receivers continues to increase we expect more revealing information relating to the details of plasma wave generation.

An alternative mechanism for the creation of the striations would be solitary waves that have been observed by FAST travelling up the magnetic field line predominately in the downward current regions adjacent to the upward current precipitating electron regions. These solitary waves have a measured field-aligned velocity (1000 - 5000 km/sec) that is comparable to that which is necessary to reproduce the slope of the striations observed in the AKR wideband data. The problem with this scenario is that the AKR source region is most likely the upward current region.

We do not rule out the possibility that the stripes may be generated by upward electron beams or "individual isolated bunches of particles" as has recently been proposed by *Carr et al.* [1997] for the generation of Jovian S-bursts. Similarly, as recently proposed by *Zarka et al.* [1997] for the generation of Jovian S-bursts, the emission may be the result of generation regions that are in a "charged state" awaiting a stimulus from a passing beam. In the scenario we propose, the stimulus is a wave rather than a plasma beam or bundle.

5.2 AMR

We have shown one of four examples of auroral myriametric radiation observed by PWI on board Polar as

the spacecraft traversed the nightside auroral region. The source of these emissions is at present in question. *Louarn et al.* [1994] have proposed that the source region of AMR is along the same field line that contains the AKR source region, but at a higher altitude. *Louarn et al.* further suggest that the emission is in the O-mode, and that the source region of AMR occurs for ratios of plasma frequency to gyrofrequency, $0.3 < f_p/f_{ce} < 1.0$ in accordance with the cyclotron maser instability. Recently *Hashimoto et al.* [1998] have confirmed that AMR is L-O mode, and proposed a multiple mode-conversion scheme of slow-Z (R-X) mode to fast-Z (L-X) mode to L-O mode (AMR) near the auroral density cavity wall where $f=f_p$. Thus these authors propose a non-gyroresonant source mechanism associated with the strong density gradients of the auroral cavity. For one of the four cases examined in detail, we find that the AMR source region is along a magnetic field line that can be distinct from the magnetic field line containing the AKR source. The other three cases unfortunately were inconclusive due to large statistical errors of the calculation (due to low signal strengths). Thus, while our results are consistent with the model of *Hashimoto et al.* and not with *Louarn et al.* for the case shown in Figure 4, the other 3 cases are consistent with both models. Nevertheless, the result of Figure 4 could be explained by slightly modifying the model of *Louarn et al.* to allow the AMR source free-energy electrons to be a distinct population of electrons from that generating the AKR.

We conclude that for one example of AMR, the source region appears to be located along a field line that is distinct from that containing the AKR source region, and may be associated with regions of strong density gradient near the edges of the auroral density cavity. This would be consistent with the conclusions of *Hashimoto et al.* [1994; 1998].

Acknowledgments. We would like to thank J. Hospodarsky for typesetting the manuscript. This work was funded by NASA grant NAS5-30371.

References

Benson, R. F., et al., Ordinary mode auroral kilometric radiation fine structure observed by DE-1, *J. Geophys. Res.*, *93*, 7515, 1988.

Boyd, T. J. M., and J. J. Sanderson, *Plasma Dynamics*, Barnes and Noble, Inc., New York, N. Y., 1969.

Carr, T. D., et al., Recent results from the University of Florida group from low-frequency radio observations of Jupiter and Neptune, in *Planetary Radio Emissions IV*, ed. by H. O. Rucker, S. J. Bauer, and A. Lecacheux, p. 25, Austrian Academy of Sciences, Austria, 1997.

Calvert, W., DE-1 measurements of AKR wave directions, *Geophys. Res. Lett.*, *12*, 381, 1985.

Filbert, P. C., and P. J. Kellogg, Electrostatic noise at the plasma frequency beyond the Earth's bow shock, *J. Geophys. Res.*, *84*, 1369, 1979.

Gurnett, D. A., et al., Initial results from the ISEE 1 and 2 plasma wave investigation, *Space Sci. Rev.*, *23*, 103, 1979.

Gurnett, D. A., and R. R. Anderson, The kilometric radio emission spectrum: Relationship to auroral acceleration processes, in *Physics of Auroral Arc Formation, Geophys. Monogr. Ser.*, *25*, edited by S.-I. Akasofu, and J. R. Kan, p. 341-350, AGU, Washington, D.C., 1981.

Gurnett, D. A., et al., Correlated low-frequency electric and magnetic noise along the auroral field lines, *J. Geophys. Res.*, *89*, 8971, 1984.

Hashimoto, et al., Auroral myriametric radiation observed by GEOTAIL, *Geophys. Res. Lett.*, *21*, 2927, 1994.

Hashimoto, K., S. Kudo, and H. Matsumoto, Source of auroral myriametric radiation observed with GEOTAIL, in press, *J. Geophys. Res.*, 1998.

Lin, C. S., et al., Excitation of low-frequency waves by auroral electron beams, *J. Geophys. Res.*, *94*, 1327, 1989.

Louarn, P., et al., Correlation between terrestrial myriametric and kilometric radio bursts observed with Galileo, *J. Geophys. Res.*, *99*, 23541, 1994.

McFadden, J. P., et al., Electron modulation and ion cyclotron waves observed by FAST, *Geophys. Res. Lett.*, *25*, 2045, 1998.

Mellott, M. M., et. al., DE-1 observations of ordinary mode and extraordinary mode auroral kilometric radiation, *Geophys. Res. Lett.*, *11*, 1188, 1984.

Melrose, D. B., A phase-bunching mechanism for fine structures in auroral kilometric radiation and Jovian decametric radiation, *J. Geophys. Res.*, *91*, 7970, 1986.

Menietti, J. D., et al., Discrete, stimulated auroral kilometric radiation observed in the Galileo and DE-1 wideband data, *J. Geophys. Res.*, *101*, 10673, 1996.

Menietti, J. D., et al., Possible stimulated AKR observed in Galileo, DE-1, and Polar wideband data, in *Planetary Radio Emissions IV*, ed. by H. O. Rucker, S. J. Bauer, and A. Lecacheux, p. 259, Austrian Academy of Sciences, Austria, 1997.

Morioka, A., H. Oya, and S. Miyatake, Terrestrial kilometric radiation observed by satellite JIKKIKEN (EXOS-B), *J. Geomagn. Geoelectr.*, *33*, 37, 1981.

Oya, H., and A. Morioka, Observational evidence of Z and L-O mode waves as the origin of auroral kilometric radiation from the Jikiken (EXOS-B) satellite, *J. Geophys. Res.*, *88*, 6189, 1983.

Temerin, M., et al., Production of flickering aurora and field-aligned electron flux by electromagnetic ion cyclotron waves, *J. Geophys. Res.*, *91*, 5769, 1986.

Wu, C. S., and L. C. Lee, A theory of the terrestrial kilometric radiation, *Astrophys. J.*, *230*, 621, 1979.

Zarka, P., et al., On the origin of Jovian decameter radio bursts, in *Planetary Radio Emissions IV*, ed. by H. O. Rucker, S. J. Bauer, and A. Lecacheux, p. 51, Austrian Academy of Sciences, Austria, 1997.